AD-A070 111 ROME AIR DEVELOPMENT CENTER GRIFFISS AFB NY F/G 9/5
METAL GRID ANGULAR FILTERS FOR SIDELOBE SUPPRESSION,1(U)
JAN 79 R J MAILLOUX, P R FRANCHI
UNCLASSIFIED RADC-TR-79-10 NL

| OF |
AD
A070111

END
DATE
FILMED
8-79
DDC

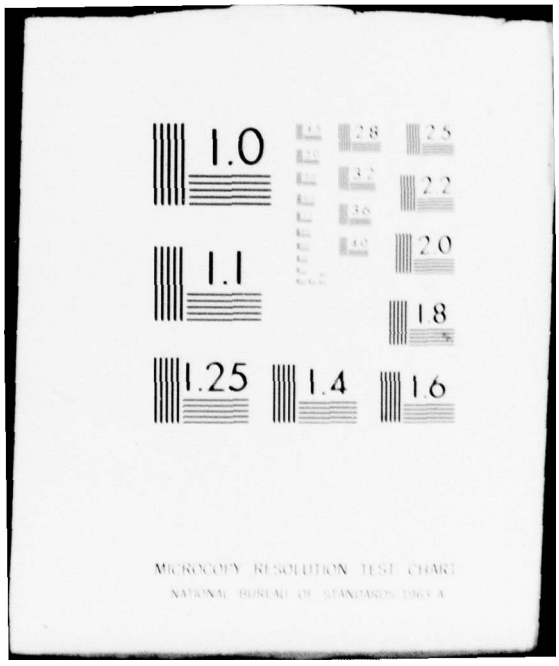
1.0
1.1
1.25
1.4
1.6
2.8
3.2
3.6
4.0
2.5
2.2
2.0
1.8
MICROCOPY RESOLUTION TEST CHART
NATIONAL BUREAU OF STANDARDS 1963 A

RADC-TR-79-10
In-House Report
January 1979

LEVEL II

METAL GRID ANGULAR FILTERS FOR SIDELOBE SUPPRESSION

Robert J. Mailloux
Peter R. Franchi

ROME AIR DEVELOPMENT CENTER
Air Force Systems Command
Griffiss Air Force Base, New York 13441

This report has been reviewed by the RADC Information Office (OI) and is releasable to the National Technical Information Service (NTIS). At NTIS it will be releasable to the general public, including foreign nations.

RADC-TR-79-10 has been reviewed and is approved for publication.

APPROVED: Walter Rotman

WALTER ROTMAN
Chief, Antennas and RF Components Branch

APPROVED: Allan C. Schell

ALLAN C. SCHELL
Chief, Electromagnetic Sciences Division

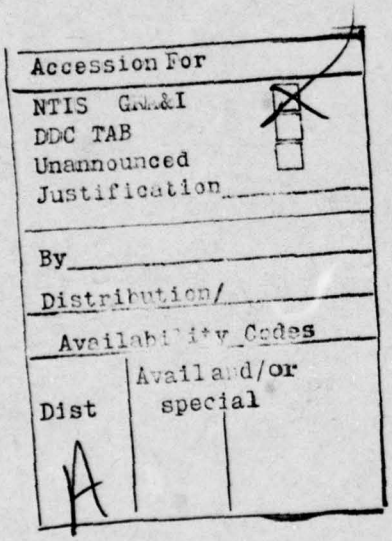

FOR THE COMMANDER: John P. Huss

JOHN P. HUSS
Acting Chief, Plans Office

If your address has changed or if you wish to be removed from the RADC mailing list, or if the addressee is no longer employed by your organization, please notify RADC (EEA) Hanscom AFB MA 01731. This will assist us in maintaining a current mailing list.

Do not return this copy. Retain or destroy.

Unclassified

SECURITY CLASSIFICATION OF THIS PAGE (When Data Entered)

REPORT DOCUMENTATION PAGE

READ INSTRUCTIONS BEFORE COMPLETING FORM

1. REPORT NUMBER: RADC-TR-79-10	2. GOVT ACCESSION NO. / 3. RECIPIENT'S CATALOG NUMBER
4. TITLE (and Subtitle): METAL GRID ANGULAR FILTERS FOR SIDELOBE SUPPRESSION	5. TYPE OF REPORT & PERIOD COVERED: In-House 6. PERFORMING ORG. REPORT NUMBER
7. AUTHOR(s): Robert J. Mailloux Peter R. Franchi	8. CONTRACT OR GRANT NUMBER(s): 16460D (11) 14
9. PERFORMING ORGANIZATION NAME AND ADDRESS: Deputy for Electronic Technology (RADC/EEA) Hanscom AFB Massachusetts 01731	10. PROGRAM ELEMENT, PROJECT, TASK AREA & WORK UNIT NUMBERS: 62702F 46001401
11. CONTROLLING OFFICE NAME AND ADDRESS: Deputy for Electronic Technology (RADC/EEA) Hanscom AFB Massachusetts 01731	12. REPORT DATE: January 1979 (11) (12) 13. NUMBER OF PAGES: 19 (12) 19p.
14. MONITORING AGENCY NAME & ADDRESS (if different from Controlling Office)	15. SECURITY CLASS. (of this report): Unclassified 15a. DECLASSIFICATION/DOWNGRADING SCHEDULE

16. DISTRIBUTION STATEMENT (of this Report)

Approved for public release; distribution unlimited.

17. DISTRIBUTION STATEMENT (of the abstract entered in Block 20, if different from Report)

18. SUPPLEMENTARY NOTES

19. KEY WORDS (Continue on reverse side if necessary and identify by block number)

Antenna
Sidelobe suppression
Low sidelobe
Angular filter

20. ABSTRACT (Continue on reverse side if necessary and identify by block number)

This report presents an analysis, design data and preliminary experimental results that demonstrate the use of metal grid angular filters for sidelobe suppression. These results indicate that sidelobe suppression in excess of 30 dB is achievable within 20° of the transmission pass band.

DD FORM 1 JAN 73 1473 EDITION OF 1 NOV 65 IS OBSOLETE

Unclassified

SECURITY CLASSIFICATION OF THIS PAGE (When Data Entered)

(20g)

JGB

309 050

Contents

Illustrations

Metal Grid Angular Filters For Sidelobe Suppression

I. INTRODUCTION

This report describes the theoretical analysis and preliminary experimental measurements of a metal grid angular filter. Previous investigations[1] have led to the development of dielectric layer filters with angle-selective properties for sidelobe suppression. A dielectric filter is composed of layers of high dielectric material separated by air spaces, and having dielectric constants chosen to provide good transmission of electromagnetic energy throughout a selected angular pass band and strong reflections for energy incident at other angles.

Dielectric filters were investigated first because of their computational simplicity. They have been shown to achieve[2, 3] 10 to 20 dB sidelobe rejection over restricted angular sections, and to behave in accordance with theoretical predictions. Unfortunately, they have a number of disadvantages that limit their

---

(Received for publication 29 January 1979)

1. Mailloux, R.J. (1976) Synthesis of spatial filters with Chebyshev characteristics, IEEE Trans. AP-24(No. 2): 174-181.
2. Mailloux, R.J., Zahn, L., Martinez, A., and Forbes, G. (1976) Multiple Mode Control of Grating Lobes in Limited Scan Arrays, RADC-TR-76-307, In House Report.
3. Pozgay, J.H., Zamoscianyk, S., and Lewis, L.R. (1976) Synthesis of Plane Stratified Dielectric Slab Spatial Filters Using Humerical Optimization Techniques, RADC-TR-76-408, Final Technical Report.

practicality. These include excessive dielectric weight and cost, fabrication difficulties in obtaining adequate mechanical tolerance, and dielectric inhomogeniety. In addition, these filters suffer from a number of features related to the electrical properties of the dielectric. These include polarization sensitivity and Brewster angle phenomena.

The obvious remedy for some of these deficiencies is to substitute metallic grids in the place of the dielectric layers. There are a number of ways in which this could be done, and indeed there is some history to the use of metallized grid structures as angular and a frequency filters. The procedure addressed in this report possesses characteristics that lead to extremely steep filter skirts and so offers excellent sidelobe control with reasonable bandwidth characteristics.

This report discusses the synthesis and analysis of metal grid filters. For the purposes of synthesis, the grids are characterized as shunt susceptances across the wavefront of some incident plane wave. Figure 1 shows a filter structure for a linearly polarized incident wave and the filter equivalent circuit. Obviously, the grid could be made of perforated metal sheets such as has been used for radome design, and the transmission line characterization and synthesis procedure would be unchanged. This equivalent circuit is used for synthesis only. The analysis of filter behavior is performed including all electromagnetic parameters. Among the features characterizing this synthesis procedure, the distinguishing feature is that it utilizes the electrical length variation of the grid separation to produce angular sensitivity, as distinguished from techniques proposed by Ortusi[4] and by Rope et al,[5] who utilize the change in grid diffraction to produce angular sensitivity. Ortusi relies upon the variability of grid diffraction as a function of angle to produce collination of an incident spherical wavefront, but the technique described here serves merely to reject incident radiation if it is outside of the prescribed transmission sector. Rope et al cascade metallic grid structures coated to obtain high transmittance at incident angles below 30^{o}, but then decreasing transmittance for greater angles. In this case, each layer is an angular filter, and the cascaded combination of layers is chosen to optimize far sidelobe suppression. The filters described in the present analysis consist of layers with relatively low broadside transmission and characterized by high normalized susceptances. The design emphasizes significant sidelobe suppression for angles well below 30^{o} as made available using the high broadside susceptances and conventional bandpass frequency filter synthesis.

---

4. Ortusi, et al (1976) U. S. Patent No. 2, 763, 860.

5. Rope, E. L., Tricoles, G., Yue, O. C. (1976) Matallic, angular filters for array economy, IEEE AP-S Intl. Symp., Digest, p 155-157.

Since the filter is entirely periodic, it does not refocus energy into the allowed angular sector, but merely rejects it. Hence, some energy is scattered back into the antenna structure, especially for reflector antennas, can result in changes to the near sidelobe structure. Care must be taken to eliminate the effects of such multiple reflections.

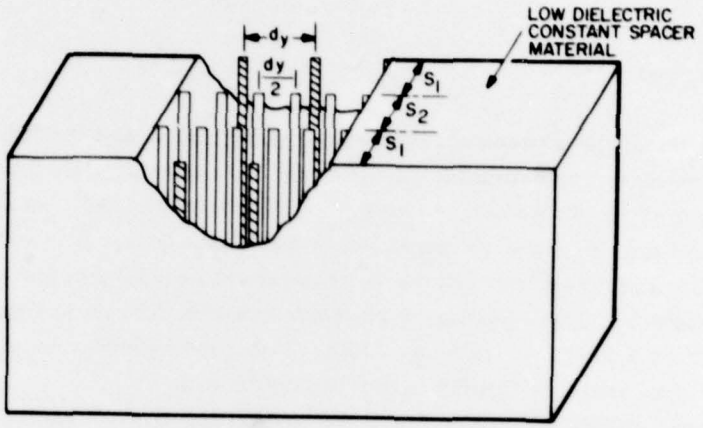

a. METAL GRID ANGULAR FILTER

Figure 1a. Metal Grid Angular Filter for Linear Polarization

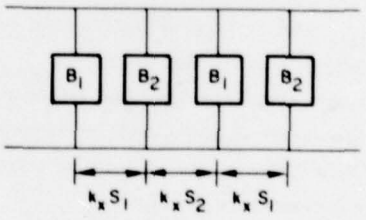

b TRANSMISSION LINE FILTER EQUIVALENT CIRCUIT

Figure 1b. Transmission Line Equivalent Circuit

2. ANALYTICAL AND THEORETICAL STUDIES

2.1 Filter Synthesis, Size and Geometry

Synthesis of the several filters described in this report is accomplished following the procedures of Matthai and Young[6] and defining the *filter propagation* constant

$$k_x = k_o \cos \eta \tag{1}$$

where η is the angle between the direction of propagation and the filter normal. At fixed frequency, selecting the angular variable to replace the usual frequency variable allows the direct use of those conventional tables and formulas to obtain a prescribed angular filter response. The end result of this procedure is a set of grid separation distances and the required shunt susceptance for the individual grid parameters. Grid dimensions are then obtained from an analysis similar to that in Section 2.2 or from tabulated data. Filter performance must be evaluated by means of an analysis similar to that of Section 2.2.

Another critical parameter is the required filter size. Clearly, the filter does not produce increased resolution beyond what would be available for the occupied aperture. The filter can be thought of as forming a subarray in the sense that if a filter is placed in front of a narrow slot aperture the slot fields would spread out throughout the filter to illuminate an extended aperture must larger than the slot. This phenomenon is related to the so-called walk-off loss[7] observed in resonators and diplexers. If the filter has a flat topped transmission characteristic out to $u_{max} = \sin \eta_{max}$, the aperture field would be roughly of the form $\sin (k_o u_{max} x)/(k_o u_{max} x)$ which has its zeros $m\lambda/2u_{max}$ apart and has the major part of its energy enclosed within the first few sets of zeros. Thus, if the filter is used in front of an aperture to suppress the sidelobe beyond the angular region bounded by u_{max}, then the filter dimensions should be equal to the aperture dimensions plus several $(\lambda/2u_{max})$ increments.

2.2 Theoretical Analysis of a Filter for Linear Polarization

The filter for a linearly polarized incident wave, as shown in Figure 1, consists of a number of metal strips arranged along the z axis. Figure 2 shows that within each grid the strips of width are equally spaced a distance d_y apart. The

6. Matthaei, G. L., Young, L., and Jones, E. M. T. (1964) Microwave Filters, Impedance – Matching Networks and Coupling Structures, McGraw Hill Book Co.

7. Arnaud, J. A., Saleh, A. A. M., Ruscio, J. T. (1974) Walk-off effects in Fabry-Perot diplexers, IEEE Trans. MTT-22(No. 5):486-493.

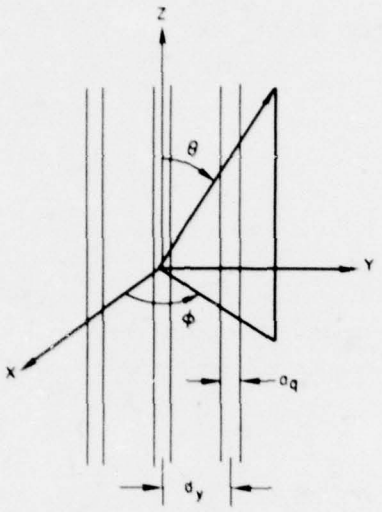

Figure 2. Coordinate System for Filter Analysis

analysis accounts for the commensurably periodic grid of Figure 1 by considering the grid with period $d_y/2$ to be a superposition of two grids, each with period d_y, displaced along the y-axis by half a period. Other grids, with more complex, but still commensurate periodicity ratios can be treated in a similar manner.

The metallic strips are aligned along the z-axis of Figure 2, with the incident field oriented along the $\hat{\theta}$ direction.

$$\overline{E}_{inc} = \hat{\theta}\, E_\theta\, e^{-j\overline{k}\cdot\overline{r}} \tag{2}$$

where $\overline{r} = \hat{x}x + \hat{y}y + \hat{z}z$ and $\overline{k} = \hat{x}k_x + \hat{y}k_y + \hat{z}k_z$

and

$$k_x = k_o \cos\eta = (\sin\theta_o \cos\phi_o)\, k_o$$

$$k_y = k_o\, u \quad = (\sin\theta_o \sin\phi_o)\, k_o$$

$$k_z = k_o\, v \quad = k_o \cos\theta_o \quad .$$

Here, u and v are the usual direction cosines. The total field is written as the sum of incident and scattered fields, with the scattered field derivable from z directed currents on the metallic strips.

$$\overline{E} = \overline{E}_{inc} - j\frac{\omega}{k_o^2}\{\nabla(\nabla\cdot\overline{A}) + k_o^2\overline{A}\}$$

$$= \overline{E}_{inc} + \overline{E}_{scat} \quad . \tag{3}$$

and

$$\overline{A} = \hat{z}\, A_z$$

The single component vector potential is derived from the sum of integrals over the various width strips. For the nth grid with period d_y and with center strip located at y_n

$$A_{z_n}(x, y, z) = \frac{1}{4\pi}\int_{-\infty}^{\infty} dz' \left\{ \sum_{p=-\infty}^{\infty} \int_{y=-a_n/2}^{a_n/2} dy' \frac{e^{-jk_o R}}{R} J_{p,n}(y') \right\} \tag{4}$$

where

$$J_{pn}(y') = J_n(y')\, e^{-j\beta_o p d_y}$$

and

$$R = \sqrt{(z - z')^2 + (x - x_n)^2 + (y - y' - y_n - pd_y)^2}$$

and

$$\beta_o = k_o u \quad .$$

The current density $J_n(y')$ is the integrated contribution across the strip thickness which is considered vanishingly small. After performing the integral and using the Poisson summation formula to transform the sum over elements at the indices "p" into a sum over modes with eigenvalues β_p, one obtains

$$A_{z_n}(x, y, z) = \frac{-e^{-jk_z z}}{2\gamma_o d_y} \int_{y'=-a_n/2}^{a_n/2} \sum_{p=-\infty}^{\infty} e^{-j\beta_p(y-y_n-y')} \frac{e^{-jK_p(|x-x_n|)}}{K_p} J_n(y') \, .$$

$$\text{for } \beta_p = \beta_o + 2\pi p\left(\frac{\lambda}{d_y}\right) \tag{5}$$

and

$$K_p = \begin{cases} \sqrt{k_o^2 - \beta_p^2 - k_z^2} & \text{for} \quad k_o^2 > \beta_p^2 + k_z^2 \\ -j\sqrt{\beta_p^2 + k_z^2 - k_o^2} & \text{for} \quad k_o^2 < \beta_p^2 + k_z^2 \end{cases}$$

Assuming constant current J_n across each strip, each of the integrals denoted above become:

$$\frac{2}{\beta_n} \sin\left(\frac{\beta_p a_n}{2}\right)$$

and the scattered field for the nth grid can be written:

$$\bar{E}_n = \frac{-\omega}{2v_o k_o^2 d_y} e^{-jk_z z} \left[\sum_{p=-\infty}^{\infty} e^{-j\beta_p y} \left(\frac{2}{\beta_p} \sin \beta_p \frac{a_n}{2}\right) \frac{e^{-jK_p|x-x_n|}}{K_p} \cdot \right.$$

$$\left. J_n e^{j\beta_p y_n} (\text{sgn}(x_n - x)\, k_z K_p \hat{x} - \beta_p k_z \hat{y} + (k_o^2 - k_z^2)\hat{z}) \right] . \qquad (6)$$

where

$$\text{sgn}(x_n - x) = 1 \qquad x_n > x$$

$$= -1 \qquad x_n < x$$

The total field is the incident field added to the sum of fields due to each grid as written in Eq. (3) with

$$\bar{E}_{scat} = \sum_n \bar{E}_n \quad . \qquad (7)$$

For thin strips the current is primarily directed in the $\hat{z}$ direction and can be found from a solution of the integral equations obtained by equating the total E_z to zero on each strip. After multiplying this set of equations by $\exp(j\beta_o y')$ and integrating the equation at the mth strip over the region $-a_m/2 \le y' \le a_m/2$, one obtains the set of M equations

$$[C]\{J\} = \{e\} \qquad (8)$$

where

$$C_{mn} = -G \sin\theta \sum_{p=-\infty}^{\infty} \left\{ \frac{e^{-jK_p|x_m - x_n|}}{K_p} \cdot \left[\frac{2}{\beta_p} \sin \frac{\beta_p a_n}{2} \right] e^{j\beta_o y_n} \right.$$

$$\left. e^{j\frac{2\pi p}{d_y}(y_n - y_m)} \frac{\sin\left(\frac{\pi p a_m}{d_y}\right)}{\left(\frac{\pi p a_m}{d_y}\right)} \right\} .$$

where

$$e_m = e^{-j(k_x x_m + \beta_o y_m)}$$

and

$$G = \frac{\omega}{2v_o d_y} = \frac{9 k_o^2}{f d_y}$$

for "f" in GHz.

The infinite sum over spatial harmonics (p) was truncated after taking enough terms to assure convergence. Experience revealed that 41 modes was adequate for all of the data used in this paper. After solving this matrix equation for the M values J_n, one can express the filter transmission coefficient as the ratio of the E_θ component in those terms of the total field that propagation in the $\hat{k}$ direction:

$$T = 1 + G \sin\theta \sum_n \left(\frac{2}{\beta_o} \sin \beta_o \frac{a_n}{2} \right) \frac{e^{+jK_o|x_n|}}{K_o} J_n e^{j\beta_o y_n} . \qquad (9)$$

The power transmission is $20 \log_{10}|T|$.

This transmission coefficient has not included any projection factor because it is assumed that factor is included in the antenna pattern or array element factor.

Note that it is possible to place several grids at the same value x_n. When this is done the values y_n and strip widths a_n are chosen so that the strips do not overlap.

Equations (8) and (9) are used to derive all of the analytical results given in the next sections.

2.3 Numerical and Experimental Studies of Filter Behavior

The final step in the synthesis process is determination of a metal strip geometry to present a specified shunt susceptance to the incident waves. Figure 3 shows the susceptance of a single grid computed using the analysis of the last section, for a grid with various strip widths "a" and periods "d_y". These curves are used to select the proper susceptances subject to the condition that all grids have the same period or, as in the case studied in the experiment, have commensurate periods. The chosen four grid filter example uses equal strip widths for each grid and the two central grids have a period one half that of the outer grids. For the purpose of computing filter performance using Eqs. (8) and (9), this filter is considered a six grid design with two grids displaced half a period to effectively half the period of the central grids.

Input data, normalized to wavelength, are given below

$a_1 = 0.0315$	$x_1 = 0.0$	$y_1 = 0.0$
$a_2 = 0.0315$	$x_2 = 0.453$	$y_2 = 0.0$
$a_3 = 0.0315$	$x_3 = 0.453$	$y_3 = 0.0933$
$a_4 = 0.0315$	$x_4 = 0.934$	$y_4 = 0.0$
$a_5 = 0.0315$	$x_5 = 0.934$	$y_5 = 0.0933$
$a_6 = 0.0315$	$x_6 = 1.387$	$y_6 = 0.0$

Figure 3 shows that the normalized susceptances for inner and outer grids is -13 and -4, respectively.

The transmission properties of this filter including inter-grid coupling and diffraction are shown in Figure 4 as a function of the conventional direction cosines along the z-axis (v) and the y-axis (u). For the given incident wave, the filter transmission is linearly polarized and almost perfectly circular in u, v space down to 30 dB rejection. This symmetry illustrates that although this computation includes diffraction, these effects are nearly negligible for the present filter. In addition, the results show that the broadside susceptance is adequate for the purposes of synthesis. Figure 5 shows preliminary measured characteristics of the filter in front of a small horn antenna. In this case the horn has such a wide element pattern (shown dotted) that the directional pattern is, in effect, the angular transmission characteristic of the filter. The dashed curve is radiation through and around a filter that has no absorber to contain the direct radiation from the waveguide feed. This figure demonstrates that the filter reflects most of the energy incident at angles corresponding to its stop band, and that most of this radiation can be suppressed by addition of absorbing material that surrounds the source antenna and filter edges. The filter represented in Figure 5 is approximately three feet square and about three inches thick at x-band. The insertion loss without absorber, averages approximately 1/2 dB. Addition of the absorber increased this loss somewhat because it intercepts some of the edge rays.

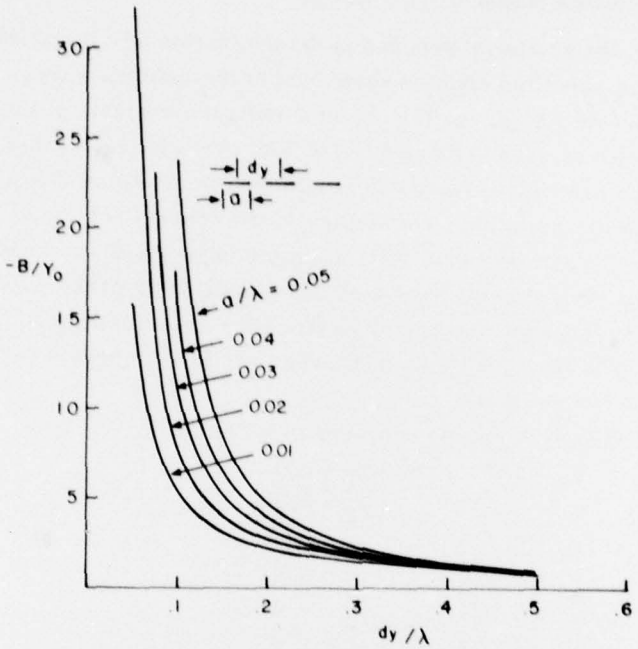

Figure 3. Normalized Susceptance for a Single Grid

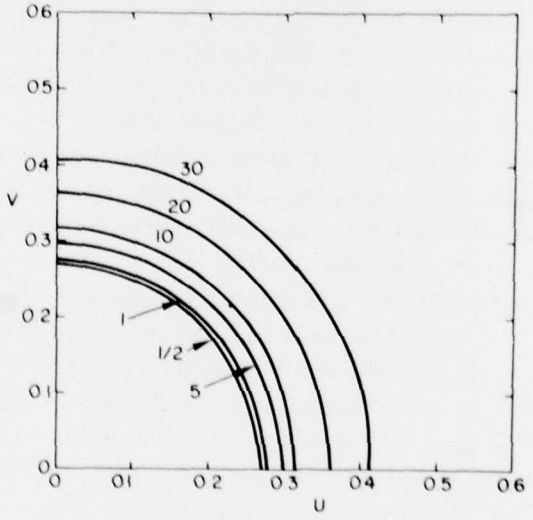

Figure 4. Filter Characteristics in Direction Cosine Space

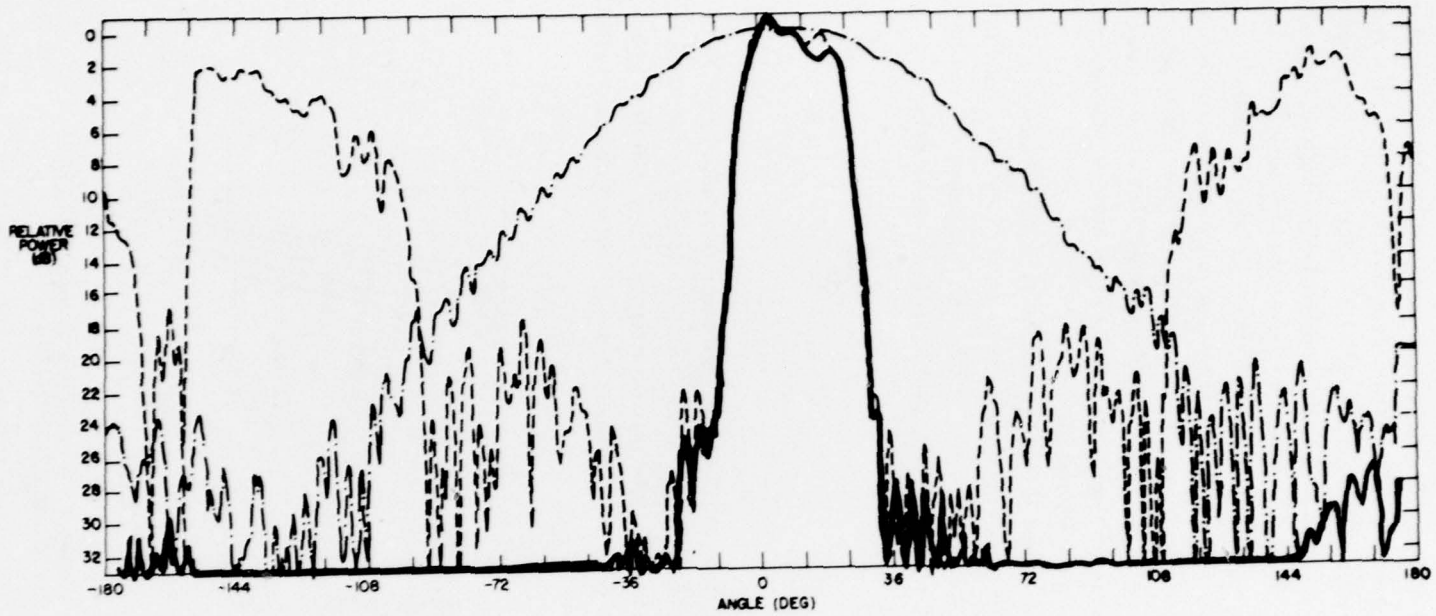

Figure 5. Filter Transmission/Reflection Characteristics at 9.7 GHz (Large Filter)

These results are quite preliminary because the filters were separated using polyfoam sheets, and it was difficult to maintain constant spacings across the entire filter. The resulting filter characteristics are thus somewhat dependent upon the lateral position of the feed horn, and the data of Figure 5 shows a resulting loss of symmetry. These results are exaggerated because the extremely high-Q design of this filter has imposed a flatness constraint on the central dielectric layer of about 0.03 inches. The severe characteristics were chosen in order to illustrate filter performance most dramatically, but they have made the design quite sensitive to inter-grid spacing. Resulting filter skirts are indeed extremely steep, and the solid curve of Figure 5 shows over 30 dB sidelobe suppression within 20° of the transmission pass band.

Figure 6 shows the effect of varying frequency and indicates that the main result is to broaden or narrow the angular pass band. The pass band is broadest at the highest frequency and narrowest at the lowest frequency. The percentage bandwidth for an idealized filter with a flat response characteristic out to η_{max} at the highest frequency is given by:

$$\frac{\Delta f}{f_{max}} = (1 - \cos \eta_{max}) \quad . \tag{10}$$

Figure 7 shows the sidelobe suppression characteristics of an 18 X 36 inch filter in front of a 12" distorted parabola at 9.3 GHz. In this case the filter is much smaller than the previous one, and so has insertion loss of 2 dB instead of the 1/2 dB indicated in the horn experiment. This loss is not due to dissipation in the

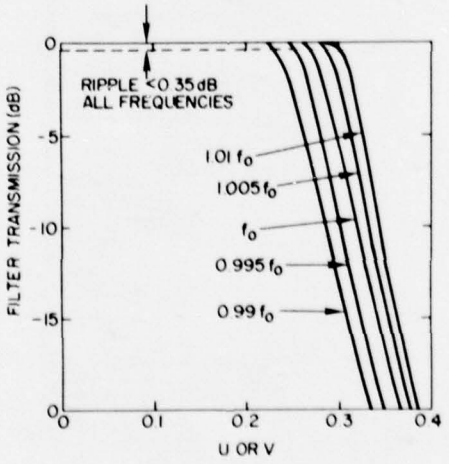

Figure 6. Frequency Dependence of the Filter Characteristics

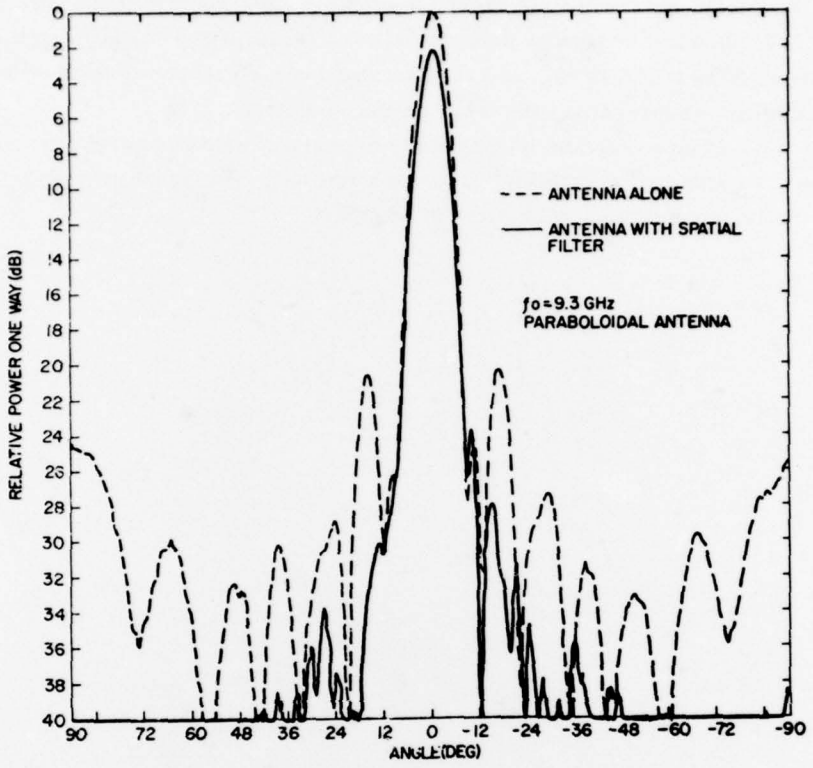

Figure 7. Radiation Characteristics of Distorted Parabola and Small Filter

filter, which is on the order of several tenths of a dB, but instead results from the finite filter size and truncation of the aperture illumination as indicated in Section 1, combined with the effects of tolerance errors.

The parabola is a far larger aperture than the previous horn feed, and the resulting pattern of the parabola in combination with the filter clearly demonstrates sidelobe reduction. To date, there is no comparable data for the larger filter which is still in an early stage of development.

3. CONCLUSION

This report has presented theoretical and experimental data showing the sidelobe suppression properties of metallic grid angular filters. The procedure for filter design is briefly described and is essentially equivalent to the synthesis of waveguide bandpass filters with inductive susceptance elements. The report

presents an analysis for multiple layer filters with equal or commensurate periodicities. Experimental results demonstrate the feasibility of filter design and construction using metal grids, and suggest that such structures can provide substantial sidelobe suppression over wide angular regions.

This work is on-going and its present emphasis is on developing a stable geometrical configuration with high tolerance constant inter-grid spacing to eliminate the transverse variation of filter parameters.

References

1. Mailloux, R.J. (1976) Synthesis of spatial filters with Chebyshev characteristics, IEEE Trans. AP-24(No. 2):174-181.

2. Mailloux, R.J., Zahn, L., Martinez, A., and Forbes, G. (1976) Multiple Mode Control of Grating Lobes in Limited Scan Arrays, RADC-TR-76-307, In House Report.

3. Pozgay, J.H., Zamoscianyk, S., and Lewis, L.R. (1976) Synthesis of Plane Stratified Dielectric Slab Spatial Filters Using Humerical Optimization Techniques, RADC-TR-76-408, Final Technical Report.

4. Ortusi, et al (1976) U.S. Patent No. 2,763,860.

5. Rope, E.L., Tricoles, G., Yue, O.C. (1976) Metallic, angular filters for array economy, IEEE AP-S Intl. Symp., Digest, p 155-157.

6. Matthaei, G.L., Young, L., and Jones, E.M.T. (1964) Microwave Filters, Impedance - Matching Networks and Coupling Structures, McGraw Hill Book Co.

7. Arnaud, J.A., Saleh, A.A.M., Ruscio, J.T. (1974) Walk-off effects in Fabry-Perot diplexers, IEEE Trans. MTT-22(No. 5):486-493.